

Robust Adaptive Computation of a One-Dimensional \mathbf{Q} -Tensor Model of Nematic Liquid Crystals

Craig S. MacDonald*

John A. Mackenzie*

Alison Ramage*

Christopher J.P. Newton†

Abstract

This paper illustrates the use of an adaptive finite element method to solve a non-linear singularly perturbed boundary value problem which arises from a one-dimensional \mathbf{Q} -tensor model of liquid crystals. The adaptive non-uniform mesh is generated by equidistribution of a strictly positive monitor function which is a linear combination of a constant floor and a power of the first derivative of the numerical solution. By an appropriate selection of the monitor function parameters, we show that the computed numerical solution converges at an optimal rate with respect to the mesh density and that the solution accuracy is robust to the size of the singular perturbation parameter.

Keywords

Nematic liquid crystals, uniform convergence, adaptive grids, mesh equidistribution, monitor function.

1 Introduction

Liquid crystals are substances which exhibit mesomorphic phases, that is, they are intermediate states of matter which occur between the crystalline solid state and the isotropic liquid state and display some of the properties of both. Different liquid crystal phases may be classified by the amount and type of orientational and positional order of molecules within a particular material. Competition between the influences of bounding surfaces and the interaction between the permanent or induced electric dipoles of the liquid crystal molecules and an applied electric field can cause the material to switch between different orientational states, with the resulting change in optical characteristics allowing the material to be used in a liquid crystal display (LCD). In recent years, the use of LCDs in consumer goods such as TVs, laptop computers, mobile phones and monitors has grown rapidly. As a result, there is increasing interest in the development of efficient simulation tools for accurately calculating the molecular orientation (and hence the optical properties) of LCDs.

One of the difficulties in liquid crystal modelling is that the underlying physical problems frequently involve characteristic length and time scales which vary by many orders of magnitude. This can cause problems in terms of designing accurate and efficient numerical simulation techniques. Typically, such issues are tackled by introducing some form of adaptive meshing, which often helps to resolve solutions with vastly different length scales accurately. In terms of liquid crystal modelling, local mesh refinement techniques such as adding additional grid points locally in regions of high error (*h*-refinement), or increasing the degree of the polynomial approximation, again based

*Department of Mathematics and Statistics, University of Strathclyde, Glasgow G1 1XH, Scotland.

†Hewlett-Packard Laboratories, Long Down Avenue, Stoke Gifford, Bristol BS34 8QZ, England.

on local errors (p -refinement), have been used with some success [10, 15, 16, 19, 23, 25, 29]. However, such methods often involve a need for complicated evolving data structures, particularly for time-dependent problems when regions requiring high spatial resolution can move throughout the domain. In this paper, we focus on moving mesh methods (r -refinement), where grid points are moved to regions of high errors while maintaining the same grid connectivity. The advantages of this approach include relatively simple implementation, comparatively easy extension of existing software for fixed mesh methods and minimal numerical diffusion and dispersion (that is, the shape and speed of time-dependent features of the solution are accurately reproduced). Comprehensive accounts of the current state-of-the-art of adaptive moving mesh methods can be found in [7, 18].

To our knowledge, the first studies of the use of moving mesh methods for liquid crystals problems were carried out by Ramage and Newton [27, 28] who considered a \mathbf{Q} -tensor description of a nematic liquid crystal. In [28], a static uniaxial 1D model was considered where the orientation depends solely on the scalar Maier-Saupe order parameter, S . Minimising the free energy density gives rise to a non-linear second-order boundary value problem for S , and an appropriate choice of boundary conditions produces a single boundary layer. A series of calculations were performed in [28] for a range of liquid crystal cell sizes, assuming fixed material properties. Therefore, while the boundary layer thickness remained constant for these experiments, the proportion of the cell covered by the boundary layer decreased as the size of the domain increased thus making the numerical computation using a fixed number of elements more challenging. The non-uniform mesh used in [28] was obtained using a well-known technique of equidistributing a positive monitor function across the available mesh elements. The monitor function considered was a scaled solution arc-length (AL); a popular monitor function which has been used previously to generate solution adaptive grids for steady and time-dependent problems [6, 17, 20, 26]. The computations in [28] indicate that solution adaptive meshes can help deliver accurate numerical results over a range of different sized domains and that the solution accuracy far exceeds that obtainable using uniform meshes with the same number of elements. The AL monitor function has subsequently been used to solve a one-dimensional, time-dependent problem describing the order reconstruction of a nematic liquid crystal inside a π -cell submitted to an electric field [27].

While the calculations in [28] highlight the potential use of adaptive mesh methods to solve problems in liquid crystals, a careful examination of the results reveals that the accuracy of the computed solutions deteriorates as the size of the domain increases using a fixed number of mesh elements. In addition, the optimal rate of convergence expected using linear and quadratic finite elements is not obtained when the domain is sufficiently large and a relatively small number of mesh elements are used. In this sense the accuracy of the adaptive method is not robust to changes in the parameters defining the problem, which is clearly undesirable.

In this paper we consider the use of solution adaptive meshes which are obtained by equidistribution of an alternative monitor function which has been used to solve linear singular perturbation problems by Beckett and Mackenzie (BM) [4, 5]. The BM monitor function contains few user-defined parameters and the effect of those that do appear are well understood. In particular, it has been shown that the adaptive meshes obtained by equidistribution of the BM monitor are well suited to singular perturbation problems in the sense that the solution accuracy is independent of the boundary layer thickness, in contrast to the meshes obtained by equidistribution of the AL monitor function. Here we carry out a detailed study of the comparative accuracy obtained using the AL and BM monitor functions for the non-linear \mathbf{Q} -tensor boundary value problem considered in [28], and explain in detail how the boundary layer thickness depends on the physical properties of the liquid crystal material (see §2.3). The BM monitor has also recently been used by Amoddeo *et al.* [1, 2] to solve the time-dependent order reconstruction problem considered in [27]. These authors claim that the BM monitor function produces adaptive meshes which are better suited to capturing the highly-localised behaviour of a scalar measure of biaxiality than the adaptive meshes obtained using the AL monitor. The detailed results which we present here clarify why this

improvement in accuracy is to be expected for such time-dependent problems.

The structure of the rest of this paper is as follows. We begin by introducing \mathbf{Q} -tensor modelling and the one-dimensional model problem which is studied in this paper. Using a spatial rescaling, we highlight the single perturbation nature of the model problem and discuss an asymptotic expansion of the solution in the boundary layer region. Section 3 contains an explanation of the concept of mesh equidistribution and the AL and BM monitor functions. In Section 4, we present numerical experiments using linear and quadratic finite elements which confirm that robust and optimal rates of convergence can be obtained for the 1D nematic liquid crystal cell studied.

2 A simple \mathbf{Q} -tensor model in one dimension

2.1 \mathbf{Q} -tensor theory

The most commonly-used continuum model for nematic liquid crystals is the Ericksen-Leslie theory for the nematic director, a unit vector which describes the mean molecular alignment at a point in a given sample volume (see e.g. [31] for details). Implicit in this theory are the assumptions that everywhere in the region of interest the material is uniaxial and the degree of order is constant. However, these assumptions are not always valid, for example, when modelling the core of a defect. One alternative model avoids these assumptions by using a symmetric traceless tensor, usually referred to as \mathbf{Q} , to characterise the liquid crystal alignment (see e.g. [12], §2.1.2). The second-rank tensor \mathbf{Q} is defined by

$$\mathbf{Q} = \sqrt{\frac{3}{2}} \left\langle \mathbf{u} \otimes \mathbf{u} - \frac{1}{3} \mathbf{I} \right\rangle, \quad (1)$$

where $\langle \dots \rangle$ represents the local ensemble average over the unit vectors \mathbf{u} along the molecular axes and \mathbf{I} is the identity. It has five degrees of freedom, two of which specify the degree of order, and three of which specify the angles of the principal directions.

For static problems, the equilibrium configuration of the dependent variables can be found by solving the set of differential equations which result from minimising the total free energy F of the liquid crystal sample. If it is assumed that distortions of \mathbf{Q} are small, F can be taken to depend only on \mathbf{Q} and its spatial gradients, that is, we may write

$$F = \int_V F_{bulk}(\mathbf{Q}, \nabla \mathbf{Q}) dv + \int_S F_{surface}(\mathbf{Q}) ds.$$

In this paper, we apply fixed boundary conditions (strong anchoring), so the surface energy term can be ignored in the minimisation. Taking the elastic energy up to second order in the gradient of \mathbf{Q} , the bulk energy density can be written as $F_{bulk} = F_{thermotropic} + F_{elastic} \equiv F_t + F_e$, with

$$\begin{aligned} F_t &= \frac{1}{2}A(T - T^*) \operatorname{tr} \mathbf{Q}^2 - \frac{\sqrt{6}}{3}B \operatorname{tr} \mathbf{Q}^3 + \frac{1}{4}C(\operatorname{tr} \mathbf{Q}^2)^2, \\ F_e &= \frac{1}{2}L_1(\operatorname{div} \mathbf{Q})^2 + \frac{1}{2}L_2|\nabla \times \mathbf{Q}|^2, \end{aligned} \quad (2)$$

where A , B , C , L_1 and L_2 are positive constants, T represents temperature and T^* is the pseudo-critical temperature at which the isotropic phase becomes unstable (see [13]). The thermotropic coefficients, A , B and C can be measured (see [9]), while the elastic constants, L_1 and L_2 are obtained by using the connection between the more traditional Frank-Oseen director-based free energy density and the \mathbf{Q} -tensor representation (see e.g. [22]).

We have a set of five coupled partial differential equations to solve to obtain the equilibrium configuration of the five dependent variables. This is a challenging problem and hence for these initial investigations we consider a simplified example which still poses significant numerical challenges because of the different characteristic lengths in the problem.

2.2 The model problem

We now introduce the model problem which we will study in depth for the remainder of the paper. We use Cartesian co-ordinates and consider a liquid crystal sample confined between two infinite horizontal plates a distance d apart. We assume that the anchoring on the plates is fixed and that the problem is “one-dimensional”, by which we mean that the \mathbf{Q} -tensor varies only in the z -direction, and is independent of x and y . We define the physical domain as $\Omega_p \equiv z \in [0, d]$.

We assume that the material is uniaxial throughout the domain. In this case two eigenvalues of \mathbf{Q} are equal and there is a unique direction along which the material behaves isotropically (specifically, the direction of the eigenvector of the unique eigenvalue). This direction is defined by a unit vector, the nematic director \mathbf{n} , and the \mathbf{Q} -tensor can be written as

$$\mathbf{Q} = \sqrt{\frac{3}{2}} S \left(\mathbf{n} \otimes \mathbf{n} - \frac{1}{3} \mathbf{I} \right), \quad (3)$$

where $S = \langle P_2(\mathbf{u} \cdot \mathbf{n}) \rangle$ is the Maier-Saupe scalar order parameter. Here P_2 is the second Legendre polynomial and comparing (1) and (3) shows that $-1/2 \leq S \leq 1$. The factor $\sqrt{3/2}$ in (1) and (3) has been chosen such that $\text{tr } \mathbf{Q}^2 = S^2$. The thermotropic energy in (2) becomes

$$F_t = \frac{1}{2} A (T - T^*) S^2 - \frac{1}{3} B S^3 + \frac{1}{4} C S^4. \quad (4)$$

Note that the thermotropic polynomial F_t has stationary points when $dF_t/dS = 0$. Two of these are physically relevant here: $S = 0$ corresponds to the isotropic phase, and

$$S = \frac{B + \sqrt{B^2 - 4AC(T - T^*)}}{2C} \equiv S_{eq} \quad (5)$$

corresponds to the nematic phase. The clearing temperature, T_c , is the value of T at which the phase transition takes place. Here, the isotropic and nematic phases have the same thermotropic energy, that is, at $T = T_c$, $F_t(0) = F_t(S_{eq}) = 0$. From this, it can be seen that

$$A(T_c - T^*) = \frac{2B^2}{9C}. \quad (6)$$

If the temperature is high enough such that

$$T > T^+ = T^* + \frac{B^2}{4AC},$$

then the thermotropic polynomial has only one stationary point corresponding to the isotropic phase $S = 0$. A plot of the thermotropic energy polynomial is shown in Figure 1 for various values of T .

To simplify the problem even further we assume that \mathbf{n} is aligned parallel to the z -axis so that (3) takes the form

$$\mathbf{Q} = \sqrt{\frac{3}{2}} S \begin{bmatrix} -\frac{1}{3} & 0 & 0 \\ 0 & -\frac{1}{3} & 0 \\ 0 & 0 & \frac{2}{3} \end{bmatrix}.$$

\mathbf{Q} now depends only on the scalar order parameter S and, in this simplified case, the elastic energy in (2) becomes

$$F_e = \frac{1}{6} (2L_1 + L_2) \left(\frac{dS}{dz} \right)^2. \quad (7)$$

The total free energy can therefore be minimised (and hence the equilibrium configuration identified) by solving a single Euler-Lagrange equation for S , subject to suitable boundary conditions.

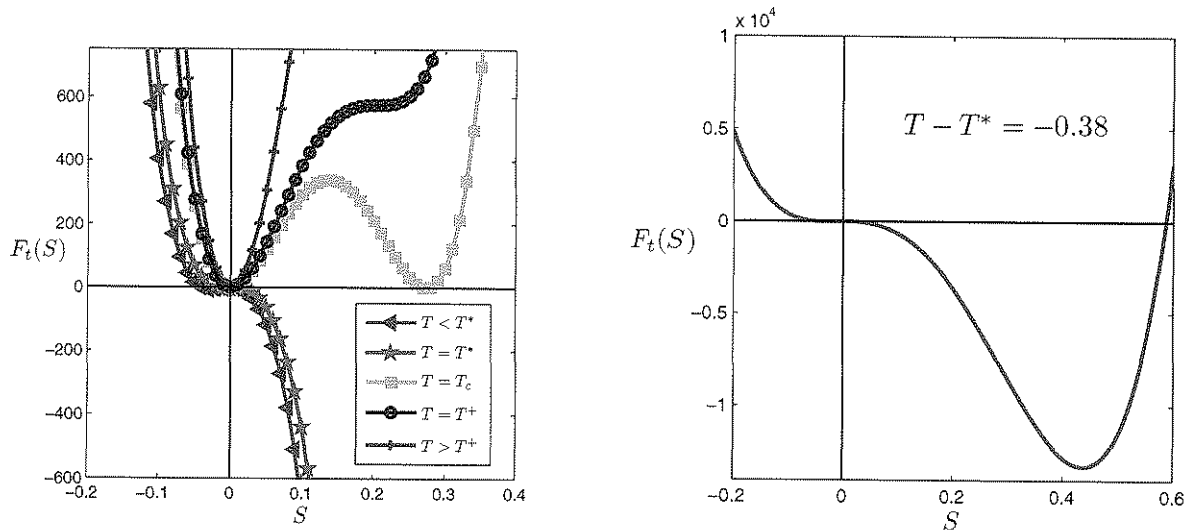


Figure 1: Thermotropic energy density F_t as a function of the scalar order parameter S .

For computational purposes, it is useful to non-dimensionalise lengths with respect to the nematic coherence length $\zeta = \sqrt{9CL_2/2B^2}$ (which is the characteristic length over which the local molecular order of the liquid crystal persists [12]). Following [30], we also make a second transformation to remove the material specific constants B and C , using relationship (6) to simplify further. Rescaling with

$$\bar{z} = \frac{1}{\zeta} z, \quad \bar{S} = \frac{3C}{2B} S,$$

our problem is now one of minimising the sum of the non-dimensional energy densities

$$\bar{F}_t = \frac{\chi}{2}\bar{S}^2 - \bar{S}^3 + \frac{1}{2}\bar{S}^4, \quad \bar{F}_e = \frac{\psi}{2\zeta^2} \left(\frac{d\bar{S}}{d\bar{z}} \right)^2, \quad (8)$$

where

$$\chi = \frac{T - T^*}{T_c - T^*}, \quad \text{and} \quad \psi = \frac{2}{3} \left(\frac{L_1}{L_2} - 1 \right) + 1.$$

For the rest of this paper, we will work with these dimensionless quantities, but will omit the overbars for ease of notation. Note that the problem domain has also been scaled in accordance with the above non-dimensionalisation; that is, we now have the scaled domain $\Omega_s \equiv z \in [0, d_s]$ when the true length of the physical domain is d (with $d = d_s\zeta$).

With this scaling, the equilibrium nematic scalar order parameter (5) becomes

$$S_{eq} = \left(3 + \sqrt{9 - 8\chi} \right) / 4.$$

When $\chi > 1$ (that is, $T > T_c$), the minimum of F_t corresponds to the isotropic phase ($S = 0$), and for $\chi < 1$, its minimum corresponds to the nematic phase ($S = S_{eq}$). There is a first-order phase transition when $\chi = 1$ ($T = T_c$). When $\chi < 0$ ($T < T^*$), the isotropic phase is unstable whereas the nematic phase is stable. The nematic phase becomes unstable when $\chi > 9/8$ ($T > T^+$).

All of our numerical experiments in §4 are carried out with $\chi \approx -0.3455$ and $\psi \approx 3.0278$. These values are commensurate with the temperatures and material constants used in [28], so the results can be directly compared. We note that for these values, the associated nematic coherence length is $\zeta \approx 4nm$ and the (scaled) equilibrium value is $S_{eq} \approx 1.6075$. This corresponds to an unscaled value of approximately 0.4396 which lies within the admissible range for the scalar order parameter.

As in the next section we will make use of results from singular perturbation analysis, we make a final scaling of the z -co-ordinate axis of z/d_s so that the computational domain is $\Omega_c \equiv z \in [0, 1]$.

With the above scalings, the governing differential equation for $S(z)$ is the Euler-Lagrange equation

$$\frac{\partial F}{\partial S} - \frac{d}{dz} \left(\frac{\partial F}{\partial S_z} \right) = 0 \quad \Rightarrow \quad \frac{\psi}{d_s^2} \frac{d^2 S}{dz^2} = \chi S - 3S^2 + 2S^3, \quad z \in (0, 1). \quad (9)$$

We solve (9) subject to the boundary conditions $S = 0$ at $z = 0$ and $S = S_{eq}$ at $z = 1$. That is, at the left edge of the domain the sample is isotropic, and at the right edge S has reached its equilibrium value of S_{eq} .

2.3 Estimates of the boundary layer component of the solution

As mentioned in the introduction, it is not immediately obvious why (9) is a singularly perturbed boundary value problem. However, if we let $\varepsilon = \sqrt{\psi}/d_s$, then (9) can be written in the more familiar form

$$-\varepsilon^2 \frac{d^2 S}{dz^2} + (\chi S - 3S^2 + 2S^3) = 0, \quad z \in (0, 1), \quad S(0) = 0 \quad \text{and} \quad S(1) = S_{eq}. \quad (10)$$

If $S_0(z)$ denotes the solution of the reduced problem which is defined by setting $\varepsilon = 0$ in (10), then

$$b(z, S_0(z)) \equiv \chi S_0 - 3S_0^2 + 2S_0^3 = 0, \quad z \in (0, 1). \quad (11)$$

As mentioned earlier, we are interested in the temperature regime $T < T^*$ and hence $\chi < 0$. Under these circumstances we can factorise $b(z, S_0(z))$ so that

$$2S_0(S_0 - \tilde{S})(S_0 - S_{eq}) = 0,$$

where $\tilde{S} < 0$. The reduced problem therefore has three constant solutions: $S_0 = 0$, $S_0 = \tilde{S}$, and $S_0 = S_{eq}$. Only $S_0 = \tilde{S}$ and $S_0 = S_{eq}$ are stable reduced solutions in the sense that for both,

$$b_S(z, S_0) = \chi - 6S_0 + 6S_0^2 > \lambda^2 > 0, \quad z \in (0, 1).$$

Clearly, the solution $S_0 = S_{eq}$ satisfies the right-hand boundary condition of the full problem (10). At the other boundary we have

$$-\int_v^0 b(z, S_{eq} + t) dt = -\int_v^0 2t(S_{eq} + t - \tilde{S})(S_{eq} + t) dt > 0, \quad \forall t \in [-S_{eq}, 0]. \quad (12)$$

The solution $S_0 = S_{eq}$ is therefore said to have a stable boundary layer at $z = 0$ [21, 24]. We seek a solution of the full problem (10) that, away from the boundary layer at $z = 0$, is close to $S_0 = S_{eq}$. Thus we may take $S_0 = S_{eq}$ as the zeroth-order smooth component in an asymptotic expansion of $S(z)$. Let $v(z)$ denote the zeroth-order boundary layer term. The following Lemma, which is equivalent to Lemma 2.3 in [21], establishes the existence of such a boundary layer term and gives bounds on its derivatives.

Lemma 2.1 *Let $\lambda_0 = \sqrt{b_S(0, S_{eq})}$. Then, for each $\delta \in (0, \lambda_0)$, there exists a positive constant C_δ such that*

$$\left| \frac{d^k v}{dz^k} \right| \leq C_\delta \varepsilon^{-k} e^{-((\lambda_0 - \delta)z/\varepsilon)}, \quad k = 0, 1, \dots, 4. \quad (13)$$

A zeroth-order asymptotic solution of (10) is therefore given by

$$S_{asym} = S_{eq}(1 - e^{-\lambda_0 z/\varepsilon}). \quad (14)$$

Using this approximate solution it is possible to get an idea of how the scaled boundary layer thickness varies in terms of the physical parameters defining our model. Here we will define the estimated boundary layer thickness as the distance z_{bl} such that $S_{asym}(z_{bl}) = \Phi S_{eq}$, where typically $\Phi \approx 0.99$. It follows from (14) that

$$z_{bl} = -\frac{\varepsilon}{\lambda_0} \ln(1 - \Phi). \quad (15)$$

We can therefore see that the scaled boundary layer thickness is an increasing function of ε . The scaled boundary layer thickness is therefore a decreasing function of the physical size of the liquid crystal cell d , but is an increasing function of the ratio of the elastic constants L_1/L_2 . The value of λ_0 depends on the temperature through the parameter χ . A plot of z_{bl} versus χ for $\varepsilon = 0.01$ ($d \approx 0.7$ microns) is shown in Figure 2 from which we can deduce that the boundary layer thickness is a increasing function of temperature.

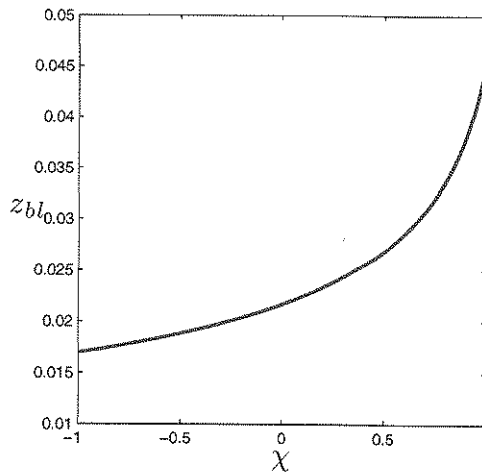


Figure 2: Variation of boundary layer thickness z_{bl} in terms of the parameter χ with $\varepsilon = 0.01$.

3 Adaptive grid generation

3.1 Grid equidistribution

Guided by the singular perturbation analysis of the previous section, we now consider the adaptive numerical solution of (10). Many adaptive grid generation techniques are based on an *equidistribution principle*. If

$$\Delta_N \equiv \{0 = z_0 < z_1 < \dots < z_{N-1} < z_N = 1\}$$

denotes a partition of the domain $\Omega_c = [0, 1]$ using N elements, and $M(z) > 0$ is a continuous function on Ω_c , then a grid is said to be equidistributed if M is evenly distributed over the mesh elements in the sense that

$$\int_{z_{i-1}}^{z_i} M(z) dz = \frac{1}{N} \int_0^1 M(z) dz, \quad i = 1, \dots, N. \quad (16)$$

The function M is referred to as the mesh density or monitor function. Many monitor functions depend on derivatives of the exact solution and hence these have to be approximated using derivatives of the numerical solution, S_N say. Furthermore, most monitor functions are not easily integrable functions and hence the practical computation of equidistributing meshes requires some form of quadrature to approximate the integrals. A simple way of finding an approximation of an equidistributed grid is to find the mesh that equidistributes a piecewise constant approximation of M , defined over a given background mesh. In particular, if

$$\Delta_N^{(k)} = \{0 = z_0^{(k)} < z_1^{(k)} < \dots < z_{N-1}^{(k)} < z_N^{(k)} = 1\}, \quad h_i^{(k)} = z_i^{(k)} - z_{i-1}^{(k)}, \quad 1 \leq i < N,$$

and $M_i^{(k)}$ is a constant on $(z_{i-1}^{(k)}, z_i^{(k)})$, then inverse linear interpolation can be used to find the mesh

$$\Delta_N^{(k+1)} = \{0 = z_0^{(k+1)} < z_1^{(k+1)} < \dots < z_{N-1}^{(k+1)} < z_N^{(k+1)} = 1\}$$

which exactly equidistributes $M^{(k)}$ in the sense that

$$\int_{z_{i-1}^{(k+1)}}^{z_i^{(k+1)}} M^{(k)} dz = \frac{1}{N} \sum_{i=1}^N M_i^{(k)} h_i^{(k)}, \quad i = 1, \dots, N.$$

Once the mesh has been updated, a new approximation S_N can be obtained using this mesh. It is then possible to define a new piecewise constant monitor function that can be used to update the mesh further. This iterative procedure is normally called de Boor's algorithm (it was used in [11] to generate solution adaptive meshes to solve two-point boundary value problems). This algorithm will form part of our iterative solution method.

The choice of an appropriate monitor function is essential to the success of the use of the equidistribution principle. In [28] the authors considered the scaled solution arc-length (AL) monitor function

$$M(S_N(z)) = \sqrt{\mu + \left(\frac{dS_N}{dz}\right)^2}, \quad (17)$$

where μ is a user-prescribed scaling parameter. Using this monitor function to solve (10), and assuming that $S_N \approx S_{asym}$, we see that, external to the boundary layer region, $dS_N/dz \approx 0$ and $M \approx \sqrt{\mu}$, whereas in the boundary layer region, $M \approx S_{eq} \varepsilon^{-1} e^{-\lambda_0 z/\varepsilon}$.

As mentioned earlier, the AL monitor function has some shortcomings when applied to the resolution of exponential-like boundary layers. We therefore consider the alternative monitor function

$$M(S_N(z)) = \alpha + \left(\left|\frac{dS_N}{dz}\right|\right)^{1/m}, \quad \text{where } \alpha = \int_0^1 \left(\left|\frac{dS_N}{dz}\right|\right)^{1/m} dz, \quad (18)$$

and m is a positive parameter. Beckett and Mackenzie (BM) used a similar monitor function to solve singularly perturbed reaction-diffusion boundary value problems using finite difference methods [4] and Galerkin finite element methods [5]. As the main difficulty in solving (10) is resolving the exponential boundary layer, where the solution first derivative is similar to the second derivative, we have, for simplicity, used the first derivative of the numerical solution in the definition of the monitor function whereas the second derivative was used in [4, 5].

The positive factor α acts as a lower bound, or floor, on the monitor function and its role is to prevent mesh starvation in areas of the domain where dS_N/dz is close to zero. For our model problem, this is the region external to the boundary layer at $z = 0$. It is important to note that α is not a user-specified parameter as its value is determined a posteriori from the numerical approximation itself. This is in contrast to the parameter μ in the definition of the AL monitor function. It has been shown in [5] that the meshes obtained by equidistribution of the BM monitor

are balanced in the sense that approximately half the available mesh elements are automatically located external to the boundary layer and the remaining half are located within the boundary layer region.

If the parameter m in (18) is greater than 1, then its effect is to smooth potentially large variations in the value of dS_N/dz . Increasing m will lead to fewer mesh elements in the boundary layer region leaving more to be deployed to cover the rest of the domain. This can potentially lead to improved accuracy for problems with boundary layers and additional solution features that need resolved in the interior of the domain. Such a situation arises in the order reconstruction problem considered in [1, 2, 3, 27]. This is one of the reasons put forward by Amoeddeo *et al.* [1, 2] for preferring the use of the BM monitor with $m = 2$, as opposed to the AL monitor function: the latter gives rise to a mesh similar to that obtained with the BM monitor function with $m = 1$.

To provide additional guidance on an appropriate choice of the parameter m to resolve a function with a boundary layer, we have the following result (equivalent to Theorem 7 from [4]).

Theorem 3.1 *Let $v(z) = e^{-(\lambda_0 z)/\varepsilon}$, and let $I_p v(z)$ denote the piecewise polynomial interpolant of $v(z)$ of degree p on each mesh element. Then, on the mesh that exactly equidistributes the BM monitor function, there exists a constant C which is independent of ε and N such that*

$$\max_{z \in [z_{i-1}, z_i]} |v(z) - I_p v(z)| < C \begin{cases} N^{-(p+1)}, & m \geq p+1, \\ N^{-m}, & m < p+1 \end{cases} \quad (19)$$

for $i = 1, 2, \dots, N$.

Therefore, to obtain the optimal rate of convergence using polynomial basis functions of degree p , it is necessary that $m \geq p+1$. In particular, if linear elements are used, then we need $m \geq 2$. This result explains why sub-optimal rates of convergence were observed using the AL monitor in [28], where both linear and quadratic elements were used. Amoeddeo *et al.* [1, 2] use quadratic elements in their simulations using the BM monitor with $m = 2$. This combination clearly would also lead to sub-optimal rates of convergence if it were used to resolve a function with an exponential boundary layer.

3.2 Adaptive solution procedure

The generation of the adaptive grid requires the global equidistribution principle (16) and the monitor function (18) be discretised. The resulting set of equations could then be coupled with the finite element discretisation of (10) to give a non-linear system for Δ_N and S_N . However, this system is large and expensive to solve, and also dictates that the grid and numerical solution be evaluated with the same level of accuracy. Thus, a popular alternative is to decouple the calculation of the grid from the finite element solution, and solve the two sets of equations in an iterative manner. Here we will use an algorithm proposed by Kopteva and Stynes [20] which is based on a modified version of the de Boor algorithm described in §3.1.

To test how close the grid is to being equidistributed at iteration k we define the two quantities

$$E_i^{(k)} = M_i^{(k)} h_i^{(k)}, \quad i = 1, \dots, N \quad \text{and} \quad I^{(k)} = \sum_{i=1}^N M_i^{(k)} h_i^{(k)}.$$

The iterative remeshing algorithm is executed until

$$\max_{1 \leq i \leq N} \{E_i^{(k)}\} \leq C_0 \frac{I^{(k)}}{N}, \quad (20)$$

where C_0 is a user defined constant. The choice of C_0 determines a balance between computational efficiency and solution accuracy. For example, with a large value of C_0 it is easier to find an approximately equidistributed grid, but this might be at the expense of solution accuracy. Conversely,

using a value of C_0 very close to one may require a large number of iterations to converge but many of these iterations will be superfluous and have very little effect on the solution accuracy. This test for convergence and guidance on suitable choices of C_0 are discussed in more detail in [8]; here we set $C_0 = 1.1$.

The overall algorithm is as follows:

1. Set the initial mesh $\Delta_N^{(0)}$ to be a uniform grid of N cells. Set the initial guess $S_N^{(0)}$ to be the linear function interpolating the boundary values $S = 0$ and $S = S_{eq}$. Set $k = 0$.
2. Obtain the finite element approximation $S_N^{(k)}$ using the mesh $\Delta_N^{(k)}$ and use Newton's method to solve the system of non-linear algebraic equations.
3. Set $h_i^{(k)} = z_i^{(k)} - z_{i-1}^{(k)}$ for each i and calculate $M_i^{(k)}$, $E_i^{(k)}$ and $I^{(k)}$.

4. If

$$\max_{1 \leq i \leq N} \{E_i^{(k)}\} \leq C_0 \frac{I^{(k)}}{N},$$

then go to Step 6. Otherwise, continue to Step 5.

5. Use the de Boor algorithm [11] to find the mesh $\Delta_N^{(k+1)}$ that equidistributes $M^{(k)}$. Set $k = k+1$ and go to Step 2.
6. Output the final mesh $\Delta_N = \Delta_N^{(k)}$ and solution $S_N = S_N^{(k)}$ and stop.

4 Numerical results

In this section we present some numerical results concerned with solving (10) using the algorithm in §3.2. Specifically, we compare computed solutions for three values of d giving boundary layers of different thicknesses, using ψ and χ as in §2.2. As the analytical solution $S(z)$ of (10) is not available in a convenient form, we have instead compared the computed solutions with the numerical solution obtained using quadratic elements and a fine non-uniform adaptive mesh which equidistributes the BM monitor function using $N = 2048$ elements. We will use $S_f(z)$ to denote this fine grid approximation to $S(z)$. The L_∞ error

$$\|e^N\|_{L_\infty(0,1)} = \max_{z \in [0,1]} |S_f(z) - S_N(z)| \quad (21)$$

has been estimated by evaluating the error at 10 evenly spaced points in each interval (z_{i-1}, z_i) , $i = 1, \dots, N$ and taking the maximum over all points. We also consider the maximum error computed at grid nodes

$$\|e^N\|_{l_\infty} = \max_{i=0, \dots, N} |S_f(z_i) - S_N(z_i)|. \quad (22)$$

Figure 3 shows a typical set of numerical results obtained for three different values of d . The examples shown have been obtained using quadratic basis functions on adaptive meshes with $N = 32$ elements using the BM monitor function with the parameter $m = 3$. In each solution plot we have also included the zeroth-order asymptotic solution S_{asym} . The vertical dotted line denotes the location of the estimated boundary layer thickness z_{bl} . We note that, for each value of d , the boundary layer nature of the solution is captured well by the adaptive meshes even though the relative boundary layer thickness decreases by an order of magnitude as we increase d . From the plots of the solution errors, we see that the errors are largest in the boundary layer region or close to the boundary layer edge. Note however that the maximum solution error is relatively insensitive to the value of d . We can also see that the computed solutions are considerably more accurate at the grid points defining the finite element mesh in comparison to the error within mesh elements.

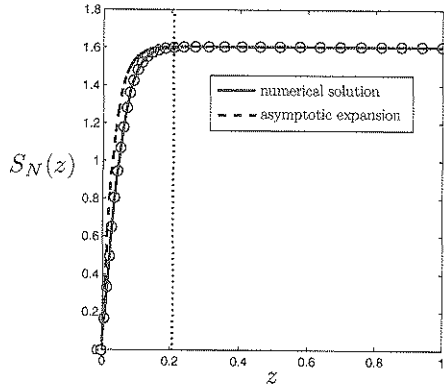
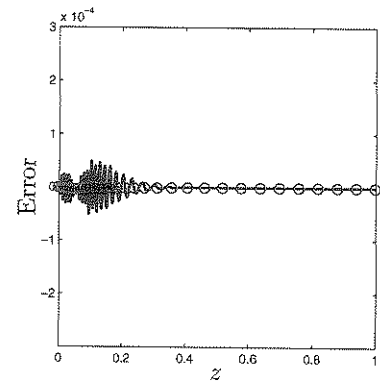
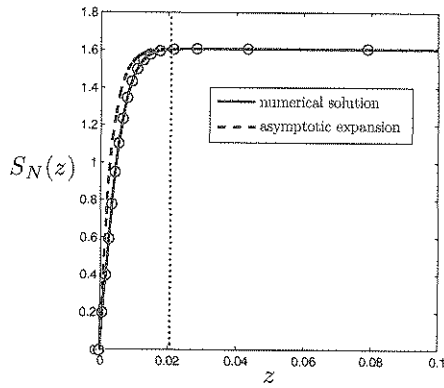
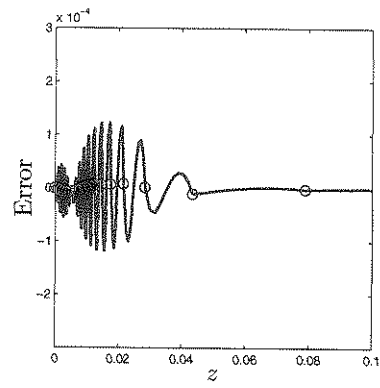
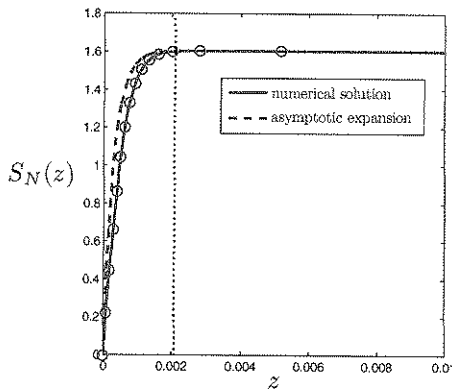
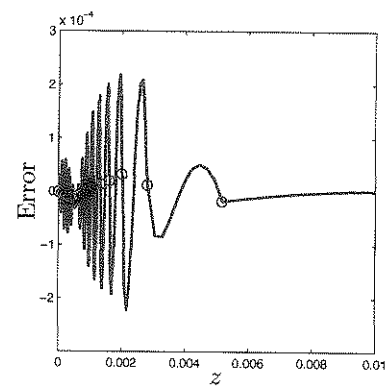
(a) Numerical solution for $d = 0.1$ microns.(b) Error for $d = 0.1$ microns.(c) Numerical solution for $d = 1$ micron.(d) Error for $d = 1$ micron.(e) Numerical solution for $d = 10$ microns.(f) Error for $d = 10$ microns.

Figure 3: Numerical solutions, estimated size of boundary layer, and errors computed with quadratic elements ($m = 3$, $N = 32$).

To quantify solution accuracy, in Table 1 we first present the L_∞ and l_∞ norms of the error obtained using linear elements and the BM monitor function with $m = 2$. The table also includes the number of iterations required for the remeshing algorithm to converge according to the condition (20) with $C_0 = 1.1$ and estimates of the rates of convergence in each norm. We observe that the L_∞ norm of the error converges at the rate $\mathcal{O}(N^{-2})$, which is the optimal rate expected using linear elements. More importantly, the accuracy obtained appears to be robust to changes in the physical size of the liquid crystal cell d . Similar uniform convergence behaviour has been established theoretically for Galerkin finite element approximations to linear reaction-diffusion problems using the BM monitor function in [5]. We can also see that the number of iterations of the remeshing algorithm required to find the adaptive mesh depends only mildly on d and N . Table 1 also shows that the maximum nodal error behaves in a similar fashion to the L_∞ error.

N	$d = 0.1$			$d = 1$			$d = 10$		
	$\ e\ _{L_\infty}$ Rate	$\ e\ _{l_\infty}$ Rate	it	$\ e\ _{L_\infty}$ Rate	$\ e\ _{l_\infty}$ Rate	it	$\ e\ _{L_\infty}$ Rate	$\ e\ _{l_\infty}$ Rate	it
8	3.172e-02	9.487e-03	2	5.224e-02	4.242e-02	10	6.632e-02	4.540e-02	25
	-	-		-	-		-	-	
16	9.703e-03	2.867e-03	2	1.300e-02	1.213e-02	6	1.490e-02	1.490e-02	22
	1.71	1.72		2.01	1.81		2.15	1.61	
32	2.818e-03	7.884e-04	1	3.398e-03	2.675e-03	3	3.670e-03	3.097e-03	110
	1.78	1.86		1.94	2.18		2.02	2.27	
64	7.044e-04	1.992e-04	1	8.057e-04	5.300e-04	3	8.161e-04	7.157e-04	20
	2.00	1.98		2.08	2.34		2.17	2.11	
128	1.733e-04	5.005e-05	1	2.024e-04	1.257e-04	4	2.120e-04	1.707e-04	3
	2.02	1.99		1.99	2.08		1.94	2.07	
256	4.291e-05	1.260e-05	1	5.073e-05	3.145e-05	2	5.231e-05	4.405e-05	4
	2.01	1.99		2.00	2.00		2.02	1.95	

Table 1: Errors, convergence rate, and iterations required (it) using linear basis functions and the BM monitor function with $m = 2$.

The analogous results obtained using quadratic elements are shown in Table 2. The convergence rate for quadratics appears to be $\mathcal{O}(N^{-3})$ in the L_∞ norm and the accuracy is again robust to changes in d . The numbers of iterations required to find the adaptive meshes are comparable to those used with linear elements. The convergence rate of the error at grid nodes appears to be $\mathcal{O}(N^{-4})$. A similar convergence rate was observed using the AL monitor function in [28]. It is well known that the finite element method can exhibit nodal superconvergence, when the numerical solution at node points is much more accurate than at intermediate points. Theoretical results in this direction go back to Douglas and Dupont [14] who showed that for linear two-point boundary value problems, the standard Galerkin approximation using polynomial elements of degree p converges in the L_∞ norm at $\mathcal{O}(N^{-(p+1)})$, whereas the solution at the grid nodes converges at $\mathcal{O}(N^{-2p})$. These convergence rates are consistent with our experiments in that there is no indication of this with linear elements, but with quadratic elements, the solution converges quicker at the grid nodes.

We now consider the effects of varying the parameter m in the BM monitor function. In Figure 4 we present the computed errors measured in the L_∞ and l_∞ norms using linear and quadratic basis functions on meshes with $N = 64$ elements and $d = 1$. We can see that the minimum error appears to occur close to $m = 2$ using linear elements and somewhere between $m = 3$ and $m = 4$ for quadratic elements. Moreover, the error increases more quickly for values of m smaller than the

N	$d = 0.1$			$d = 1$			$d = 10$		
	$\ e\ _{L_\infty}$ Rate	$\ e\ _{l_\infty}$ Rate	it	$\ e\ _{L_\infty}$ Rate	$\ e\ _{l_\infty}$ Rate	it	$\ e\ _{L_\infty}$ Rate	$\ e\ _{l_\infty}$ Rate	it
8	2.999e-03 -	1.108e-03 -	1	2.519e-02 -	1.100e-02 -	5	8.495e-02 -	8.4949e-02 -	9
16	3.221e-04 3.21	6.585e-05 4.07	1	1.376e-03 4.19	2.493e-04 5.46	5	2.864e-03 4.89	6.312e-04 7.07	11
32	5.014e-05 2.68	3.635e-06 4.18	1	1.230e-04 3.48	1.047e-05 4.57	3	2.203e-04 3.70	3.339e-05 4.24	6
64	6.026e-06 3.06	2.389e-07 3.93	1	1.612e-05 2.93	5.246e-07 4.31	2	1.882e-05 3.55	2.500e-06 3.73	10
128	7.930e-07 2.93	1.522e-08 3.97	1	1.726e-06 3.22	3.995e-08 3.71	2	2.122e-06 3.14	3.494e-07 2.83	4
256	9.819e-08 3.01	9.779e-10 3.96	1	2.119e-07 3.02	2.211e-09 4.17	2	2.538e-07 3.06	2.345e-08 3.90	3

Table 2: Errors, convergence rate, and iterations required (it) using quadratic basis functions and the BM monitor function with $m = 3$.

optimal value. Theorem 3.1 indicates that if $m \geq p + 1$, then the approximation will converge at the optimal rate with respect to N . This is consistent with our findings, namely that the optimal rates of convergence, and best approximations, are attained with $m \geq 2$ for linears and $m \geq 3$ for quadratics. Although we have presented results here only for the case $d = 1$, we observe similar behaviour when $d = 0.1$ and $d = 10$ microns.

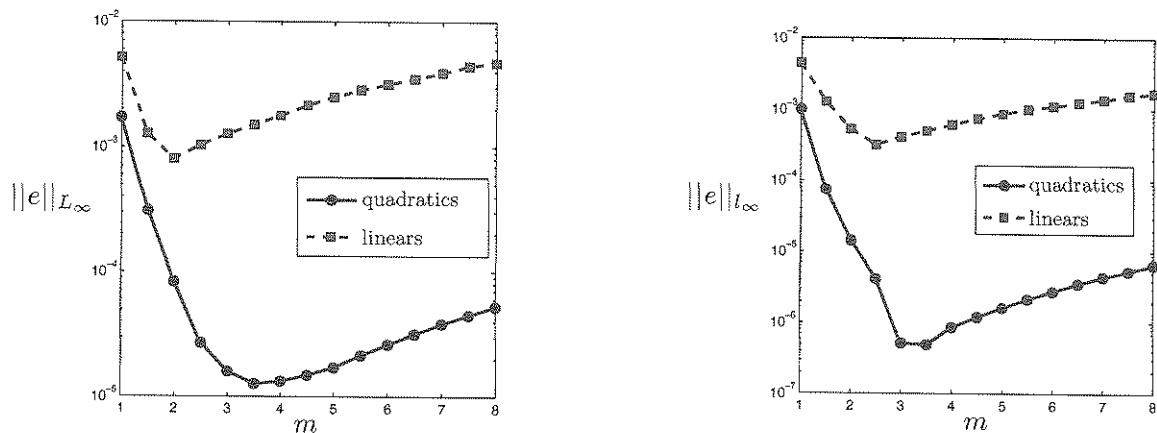
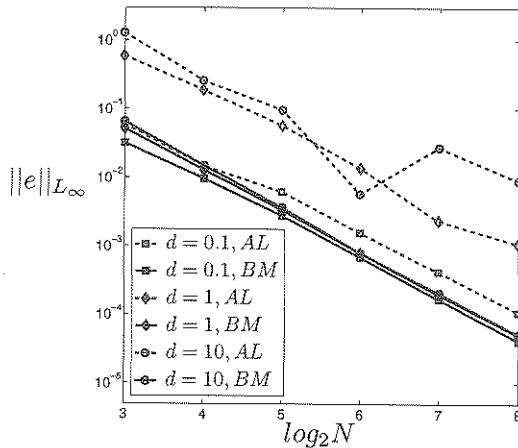


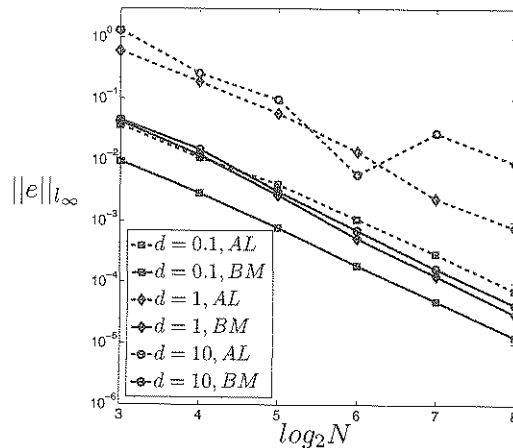
Figure 4: Error variation with respect to the parameter m in the BM monitor function.

We can also compare the accuracy obtained using the BM monitor in comparison with that obtained using the AL monitor function. Figures 5 (a) and (b) show the errors in the L_∞ and l_∞ norms with linear basis functions. It can be seen that, for all values of d , the error using the BM monitor is smaller than the error obtained using the AL monitor with the same number of mesh points. Note also that the errors using the AL monitor are very sensitive to the size of the physical domain d . In particular, we see that for a fixed number of grid points the errors increase as d is increased. Figures 5 (c) and (d) show equivalent plots for quadratic basis functions. Similar observations can be made as for the linear case, with BM outperforming AL, both in terms of

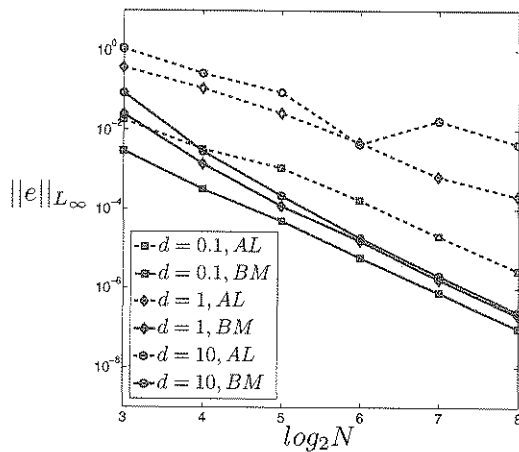
accuracy and robustness to variations in d .



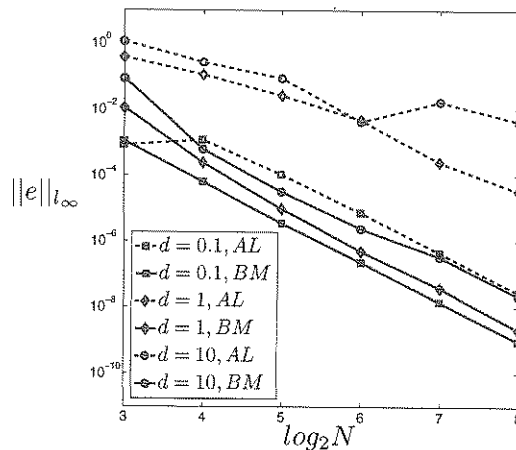
(a) Convergence of $\|e\|_{L_\infty}$ using linear elements.



(b) Convergence of $\|e\|_{l_\infty}$ using linear elements.



(c) Convergence of $\|e\|_{L_\infty}$ using quadratic elements.



(d) Convergence of $\|e\|_{l_\infty}$ using quadratic elements.

Figure 5: Comparison of accuracy obtained by equidistribution of the AL and BM monitor functions.

Having established that the use of the BM monitor function can improve accuracy (for a fixed number of grid points), we now consider the overhead associated with the computation of the adaptive grid which should be taken into account when assessing the overall efficiency of the approach. To illustrate this we look at the CPU time required using the BM and AL monitor functions to solve our problem to a given degree of accuracy in the L_∞ norm using quadratic basis functions. It has been shown that uniform meshes perform poorly in comparison to those obtained using the AL monitor function [27] and hence we will not consider uniform meshes here as they are unlikely to be competitive. The number of elements and CPU times required are listed in Table 3. The results indicate that BM outperforms AL in each case and that the relative efficiency of BM improves significantly as higher accuracy is required and as d is increased.

	AL			BM			
$d = 0.1$							
TOL	N	it	$t(s)$	N	it	$t(s)$	% speedup
1e-3	32	1	0.091922	12	1	0.082384	12
1e-5	168	1	0.410808	56	1	0.093883	338
$d = 1$							
TOL	N	it	$t(s)$	N	it	$t(s)$	% speedup
1e-3	110	2	0.321125	16	2	0.113015	184
1e-5	816	1	39.4324	100	1	0.216643	18102
$d = 10$							
TOL	N	it	$t(s)$	N	it	$t(s)$	% speedup
1e-3	166	3	8.78359	26	10	0.708193	1140
1e-5	2042	1	4483.39	88	6	3.70893	120781

Table 3: Comparison of CPU times required to produce an error in the L_∞ norm below the value TOL using quadratic elements and the AL and BM monitor functions.

5 Conclusions

In this paper we have considered the adaptive solution of a non-linear boundary value problem arising from a \mathbf{Q} -tensor model of a nematic liquid crystal. The solution-adaptive mesh is obtained by equidistribution of the BM monitor function, which has previously been used to solve linear reaction-diffusion problems. Numerical experiments have been carried out which show that the computed errors are robust to variations in the size of the liquid crystal cell size – a desirable property which is not realised when a uniform grid or an adaptive mesh based on equidistribution of the AL monitor function is used. An iterative algorithm has been used to find approximately equidistributed grids, and to obtain solutions to a given degree of accuracy. We have shown that the use of the BM monitor function can result in over a thousand fold decrease in CPU time compared to the use of the AL monitor function.

Although the results in this paper deal with a somewhat idealised model problem, they do have important implications for the solution of more realistic physical problems such as the bi-axial order reconstruction problem considered in [1, 2, 3, 27]. For this problem the full \mathbf{Q} -tensor must be used resulting in five coupled non-linear PDEs, corresponding to the components q_i , $i = 1, \dots, 5$. These equations are solved in conjunction with an equation describing the electric potential. The improvements in efficiency presented here using the BM monitor function are extremely promising and suggest that similar reductions in grid densities can be achieved for time-dependent problems in liquid crystal modelling.

6 Acknowledgment

Support for C MacDonald was provided by the EPSRC and Hewlett-Packard.

References

- [1] A. Amoddeo, R. Barberi, and G. Lombardo. Moving mesh partial differential equations to describe nematic order dynamics. *Comput. Math. Appl.*, 60:2239–2252, 2010.
- [2] A. Amoddeo, R. Barberi, and G. Lombardo. Electric field-induced fast nematic order dynamics. *Liq. Cryst.*, 38(1):93–103, 2011.
- [3] R. Barberi, F. Ciuchi, G.E. Durand, M. Iovane, D. Sikharulidze, A.M. Sonnet, and E.G. Virga. Electric field induced order reconstruction in a nematic cell. *Eur. Phys. J. E*, 13:61–71, 2004.
- [4] G. Beckett and J.A. Mackenzie. On a uniformly accurate finite difference approximation of a singularly perturbed reaction-diffusion problem using grid equidistribution. *J. Comp. Appl. Math.*, 131:381–405, 2001.
- [5] G. Beckett and J.A. Mackenzie. Uniformly convergent high order finite element solutions of a singularly perturbed reaction-diffusion equation using mesh equidistribution. *Appl. Numer. Math.*, 39:31–45, 2001.
- [6] J.G. Blom, J.M. Sanz-Serna, and J.G. Verwer. On simple moving grid methods for one-dimensional evolutionary partial differential equations. *J. Comput. Phys.*, 74:191–213, 1988.
- [7] C.J. Budd, W. Huang, and R.D. Russell. Adaptivity with moving grids. *Acta Numerica*, 18:111–241, 2009.
- [8] N.M. Chadha and N. Kopteva. A robust grid equidistribution method for a one-dimensional singularly perturbed semilinear reaction-diffusion problem. *IMA J. Numer. Anal.*, 31:188–211, 2011.
- [9] H.J. Coles. Laser and electric field induced birefringence studies of the cyano-biphenyl homologues. *Mol. Cryst. Liq. Cryst.*, 49:67–74, 1978.
- [10] S. Cornford and C.J.P. Newton. An adaptive hierarchical finite element method for modelling liquid crystal devices. Technical Report HPL-2011-143, Hewlett-Packard Laboratories, 2011.
- [11] C. de Boor. Good approximation by splines with variable knots II. In *Lecture Notes in Mathematics*, volume 363, pages 12–20. Springer-Verlag, 1974.
- [12] P. G. De Gennes and J. Prost. *The Physics of Liquid Crystals*. Clarendon Press, Oxford, 2. edition, 1993.
- [13] P.G. de Gennes. Short range order effects in the isotropic phase of nematics and cholesterics. *Mol. Cryst. Liq. Cryst.*, 129:193–214, 1971.
- [14] J. Douglas and T. Dupont. Galerkin approximations for two point boundary value problem using continuous, piece-wise polynomial spaces. *Numer. Math.*, 22:99–109, 1974.
- [15] J. Fukuda and H. Yokoyama. Director configuration and dynamics of a nematic liquid crystal around a two-dimensional spherical particle: Numerical analysis using adaptive grids. *Eur. Phys. J. E*, 4:389–396, 2001.
- [16] J. Fukuda, M. Yoneya, and H. Yokoyama. Defect structure of a nematic liquid crystal around a spherical particle: adaptive mesh refinement approach. *Phys. Rev. E*, 65(4):041709, 2002.
- [17] W. Huang, Y. Ren, and R.D. Russell. Moving mesh methods based on moving mesh partial differential equations. *J. Comput. Phys.*, 113:279–290, 1994.

- [18] W. Huang and R.D Russell. *Adaptive Moving Mesh Methods*. Springer, New-York, 2011.
- [19] R. James, E. Willman, F.A. Fernandez, and S. E. Day. Finite-element modeling of liquid-crystal hydrodynamics with a variable degree of order. *IEEE Transactions on Electron Devices*, 53(7):1575–1582, 2006.
- [20] N. Kopteva and M. Stynes. A robust adaptive method for a quasi-linear one-dimensional convection-diffusion problem. *SIAM J. Numer. Anal.*, 39:1446–1467, 2001.
- [21] N. Kopteva and M. Stynes. Numerical analysis of a singularly perturbed nonlinear reaction-diffusion problem with multiple solutions. *Comput. Math. Appl.*, 51:857–864, 2006.
- [22] H. Mori, Jr. E.C. Gartland, J.R. Kelly, and P.J. Bos. Multidimensional director modeling using the q tensor representation in a liquid crystal cell and its application to the pi cell with patterned electrodes. *Jpn. J. Appl. Phys.*, 38:135–146, 1999.
- [23] N.J. Mottram and C.J.P. Newton. Introduction to Q-tensor theory. Technical Report 10/04, University of Strathclyde, 2004.
- [24] R.E. O'Malley. *Singular perturbation methods for ordinary differential equations*. Springer-Verlag, New-York, 1991.
- [25] P. Patricio, M. Tasinkevych, and M.M. Telo da Gama. Colloidal dipolar interaction in 2D smectic-C films. *Eur. Phys. J. E*, 7:117–122, 2002.
- [26] Y. Qiu, D.M. Sloan, and T. Tang. Numerical solution of a singularly perturbed two-point boundary value problem using equidistribution: analysis of convergence. *J. Comput. Appl. Math.*, 116:121–143, 2000.
- [27] A. Ramage and C.J.P. Newton. Adaptive solution of a one-dimensional order reconstruction problem in Q-tensor theory of liquid crystals. *Liq. Cryst.*, 34(4):479–487, 2007.
- [28] A. Ramage and C.J.P. Newton. Adaptive grid methods for Q-tensor theory of liquid crystals: A one-dimensional feasibility study. *Mol. Cryst. Liq. Cryst.*, 480(1):160–181, 2008.
- [29] N.M. Silvestre, P. Patricio, and M.M. Telo da Gama. Elliptical soft colloids in smectic-C films. *Phys. Rev. E*, 74(2):021706, 2006.
- [30] A. Sonnet, A. Kilian, and S. Hess. Alignment tensor versus director: Description of defects in nematic liquid crystals. *Phys. Rev. E*, 52(1):718–722, July 1995.
- [31] I.W. Stewart. *The Static and Dynamic Continuum Theory of Liquid Crystals*. Taylor & Francis, London, 2004.